Supporting Information

Ultrasensitive, Ultrafast and Gate-Tunable Two-Dimensional Photodetectors in Ternary Rhombohedral $ZnIn_2S_4$ for Optical Neural Networks

Weili Zhen[ab§], Xi Zhou[de§], Shirui Weng[a], Wenka Zhu[a*], and Changjin Zhang[ac†]

[a]*High Magnetic Field Laboratory, Chinese Academy of Sciences, Hefei 230031, China*

[b]*University of Science and Technology of China, Hefei 230026, China*

[c]*Institutes of Physical Science and Information Technology, Anhui University, Hefei 230601, China*

[d]*The Interdisciplinary Research Center, Shanghai Advanced Research Institute, Chinese Academy of Sciences, Shanghai 201210, China*

[e]*School of Microelectronics, University of Chinese Academy of Sciences, Beijing 100049, China*

*Email: wkzhu@hmfl.ac.cn

†Email: zhangcj@hmfl.ac.cn

§W.Z. and X.Z. contributed equally to this paper

1. Figures and tables

1.1. Schematic diagram of CVT growth of R-ZIS single crystals and an optical image

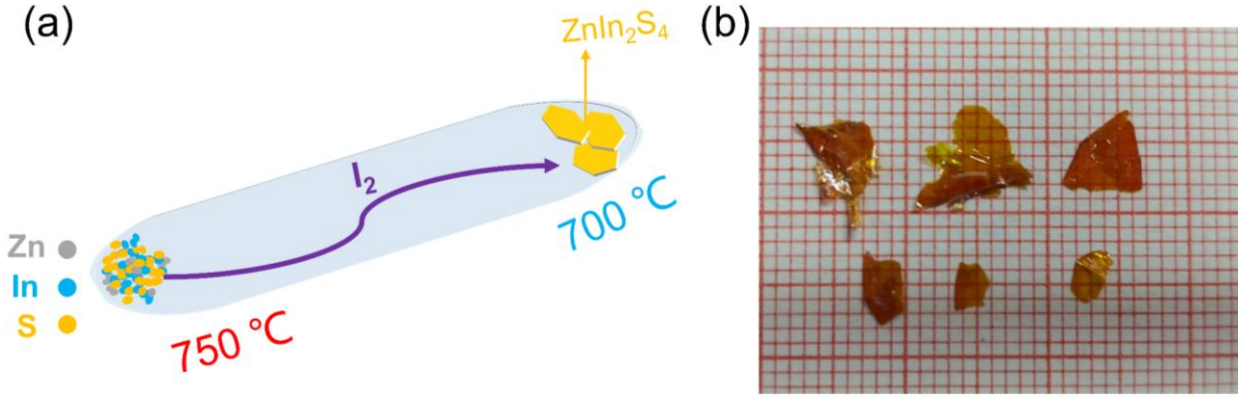

Figure S1. (a) Schematic diagram of chemical vapor transport growth of R-ZIS sing crystals. (b) An optical image of the as-grown R-ZIS single crystals. The size of each small grid is 1×1 mm^2.

1.2. Powder XRD pattern

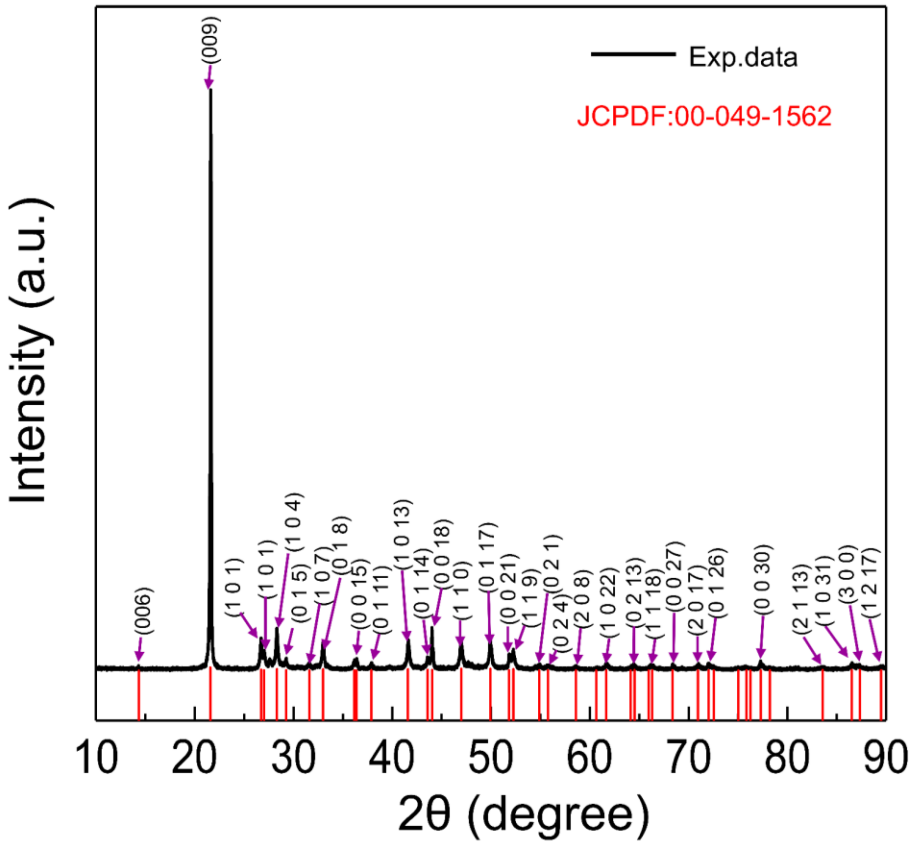

Figure S2. Powder XRD pattern of R-ZIS. The red ticks indicate the positions of the diffractions

of PDF No. 00-049-1562.

1.3. Optical image showing more R-ZIS flakes

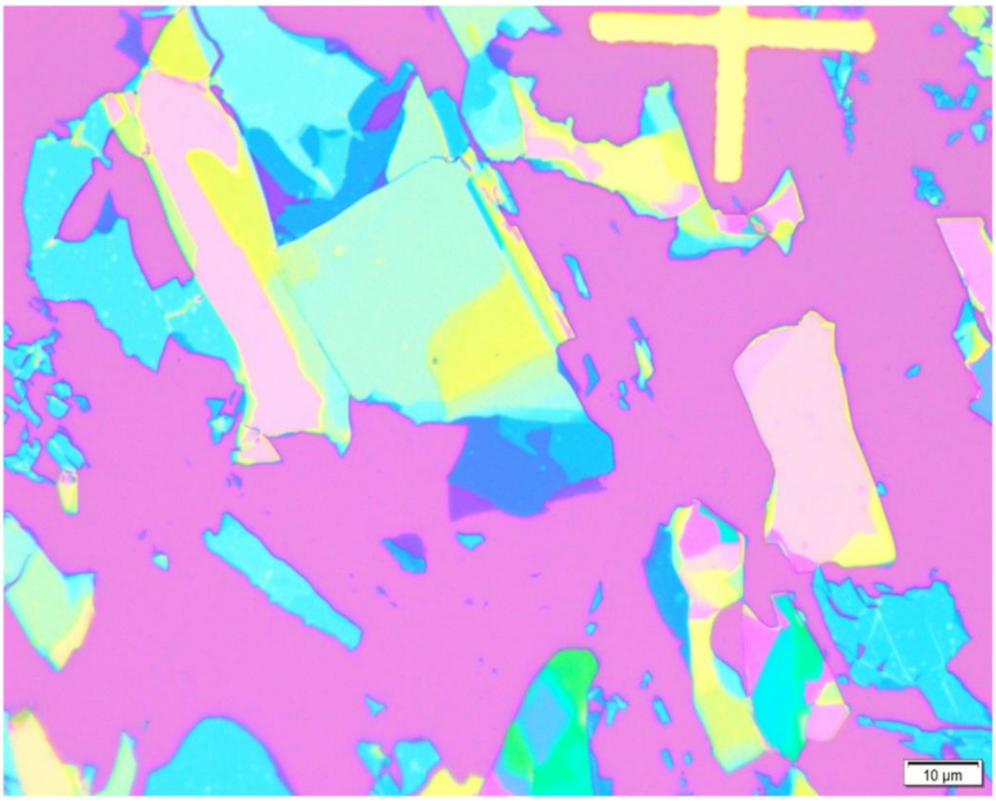

Figure S3. Optical image of R-ZIS flakes on SiO_2/Si substrate. Different optical contrasts correspond to different thicknesses and layers.

1.4. SAED pattern and HRTEM image taken on the cross section of an R-ZIS thin flake prepared by focused ion beam

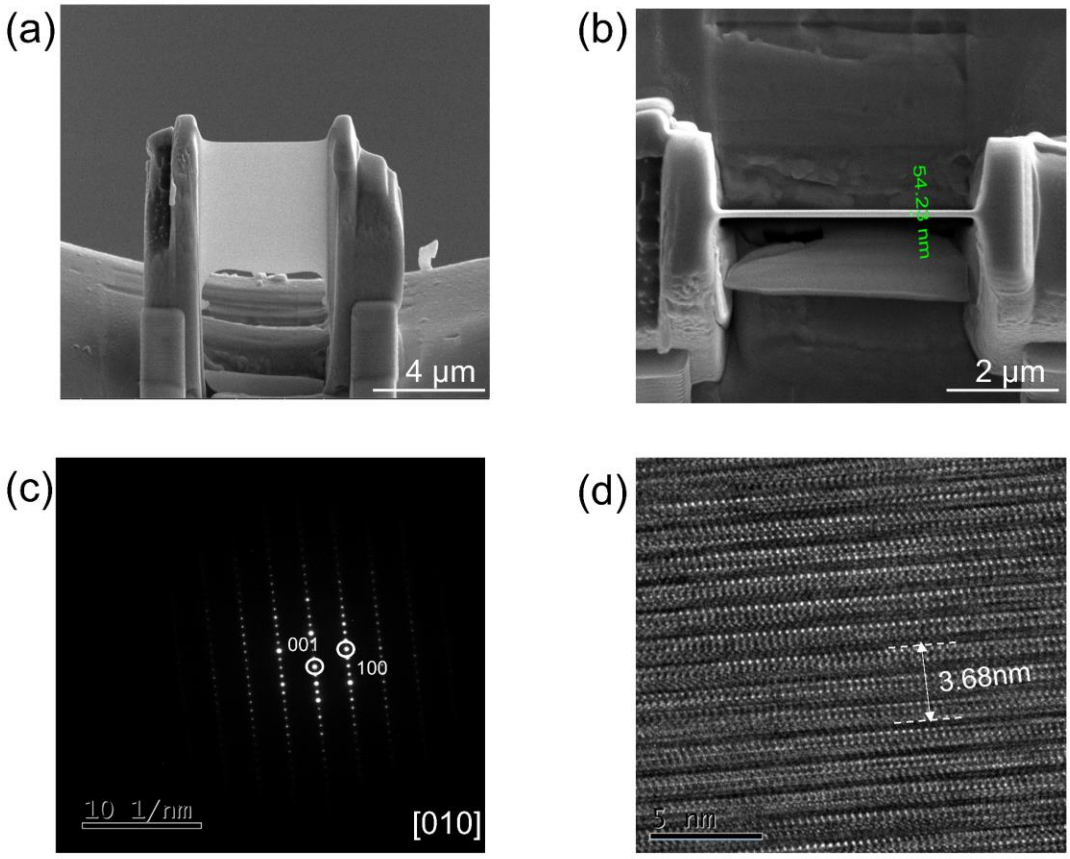

Figure S4. (a) R-ZIS thin flake prepared by focused ion beam. (b) Cross-sectional view of the R-ZIS sheet. The thickness is about 54 nm. (c) SAED pattern taken on the sample shown in (a) and (b). The diffraction spots correspond to the [001] and [100] crystallographic planes. The zone axis is [010]. (d) HRTEM image. The interplanar spacing is determined to be about 3.68 nm, which is close to the lattice parameter c = 3.7 nm.

1.5. STEM-EDX spectrum

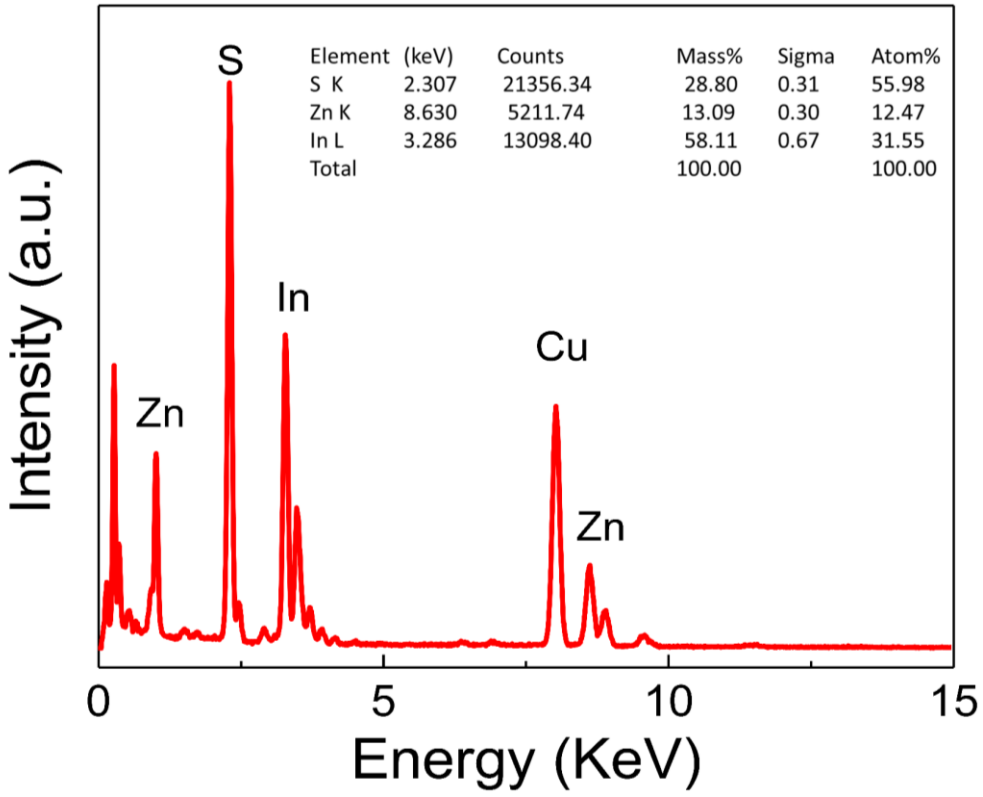

Figure S5. STEM-EDS spectrum of R-ZIS flake. The atomic ratio is close to 1:2:4.

1.6. Optical image and *I–V* curves of R-ZIS photodetector based on Cr/Au contact

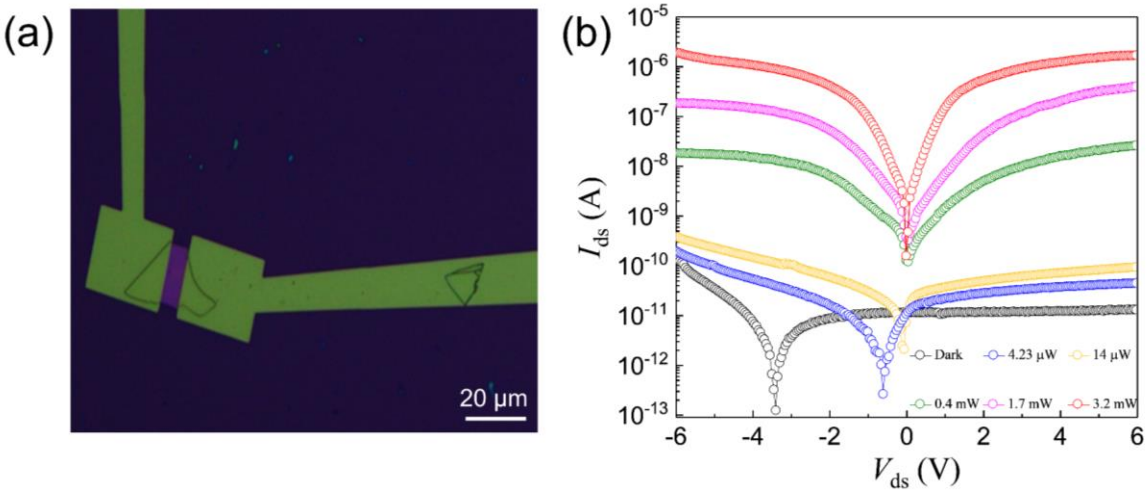

Figure S6. (a) Optical image of R-ZIS photodetector based on Cr/Au contact. The scale bar is 20 μm. (b) I_{ds}–V_{ds} characteristics taken in the dark and under a 405 nm laser tuned to different laser

powers.

1.7. Time-resolved photocurrent of R-ZIS photodetector taken under lasers of different wavelength

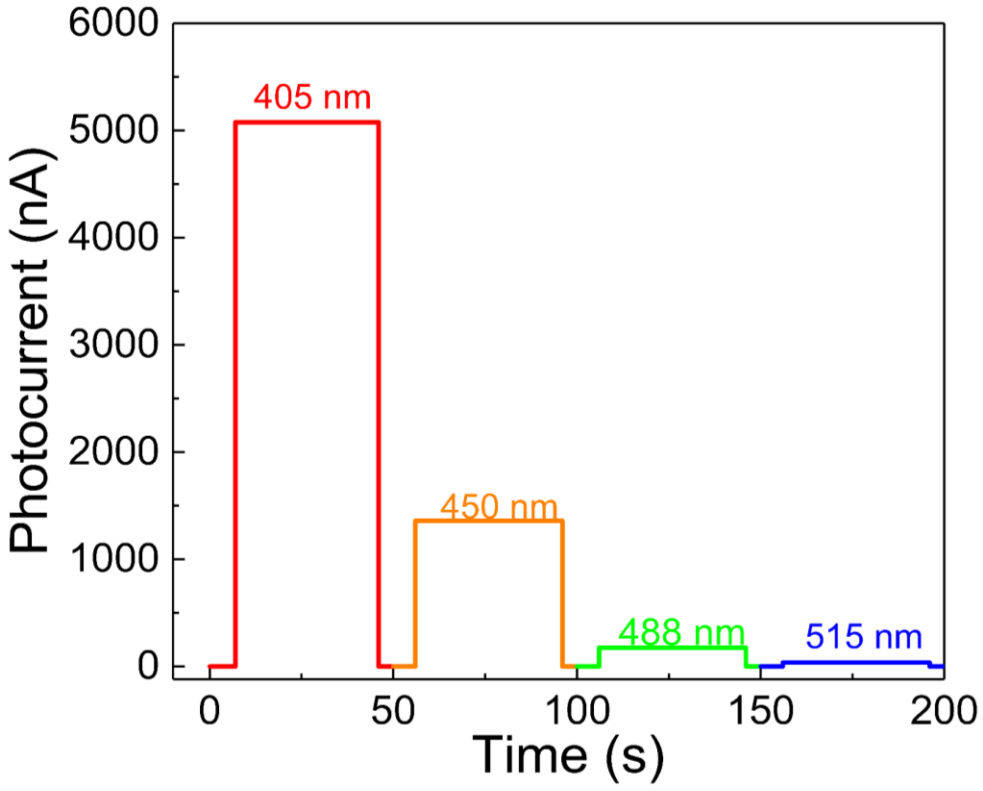

Figure S7. Time-resolved photocurrent of R-ZIS photodetector taken under lasers of different wavelength (405 nm, 450 nm, 488 nm and 515 nm) at V_{ds} = 5 V and 5.3 mW.

1.8. *I–V* curve taken under illumination of 370 nm

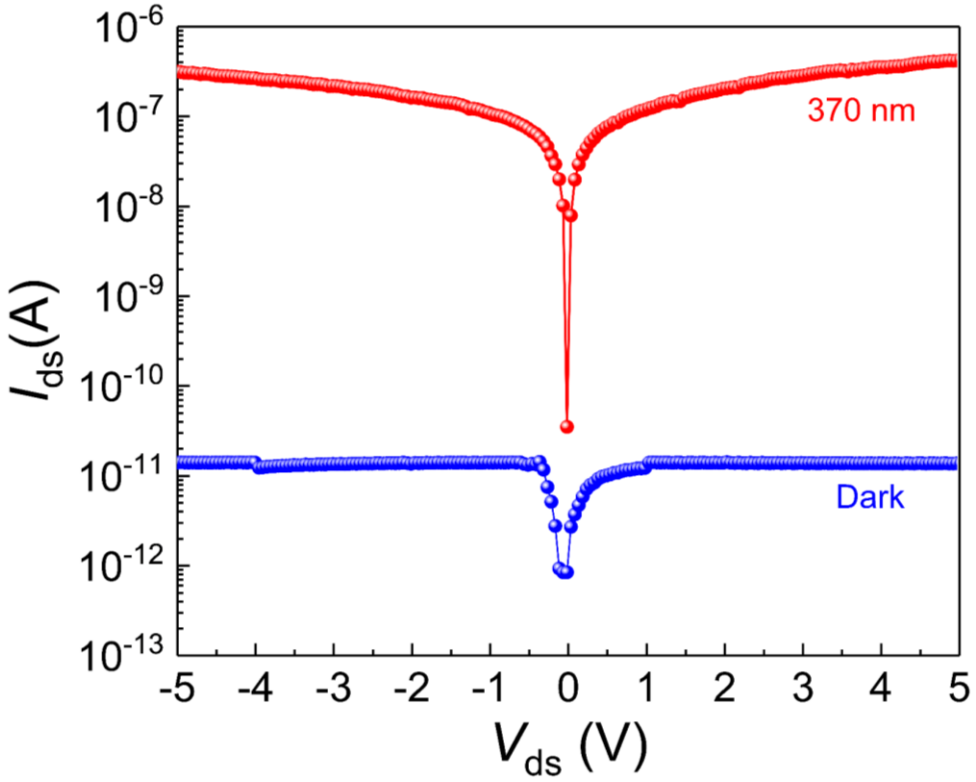

Figure S8. Semi-logarithmic I_{ds}–V_{ds} characteristics taken in the dark and under illumination of 370 nm.

1.9. Test results of more devices (S2 and S3)

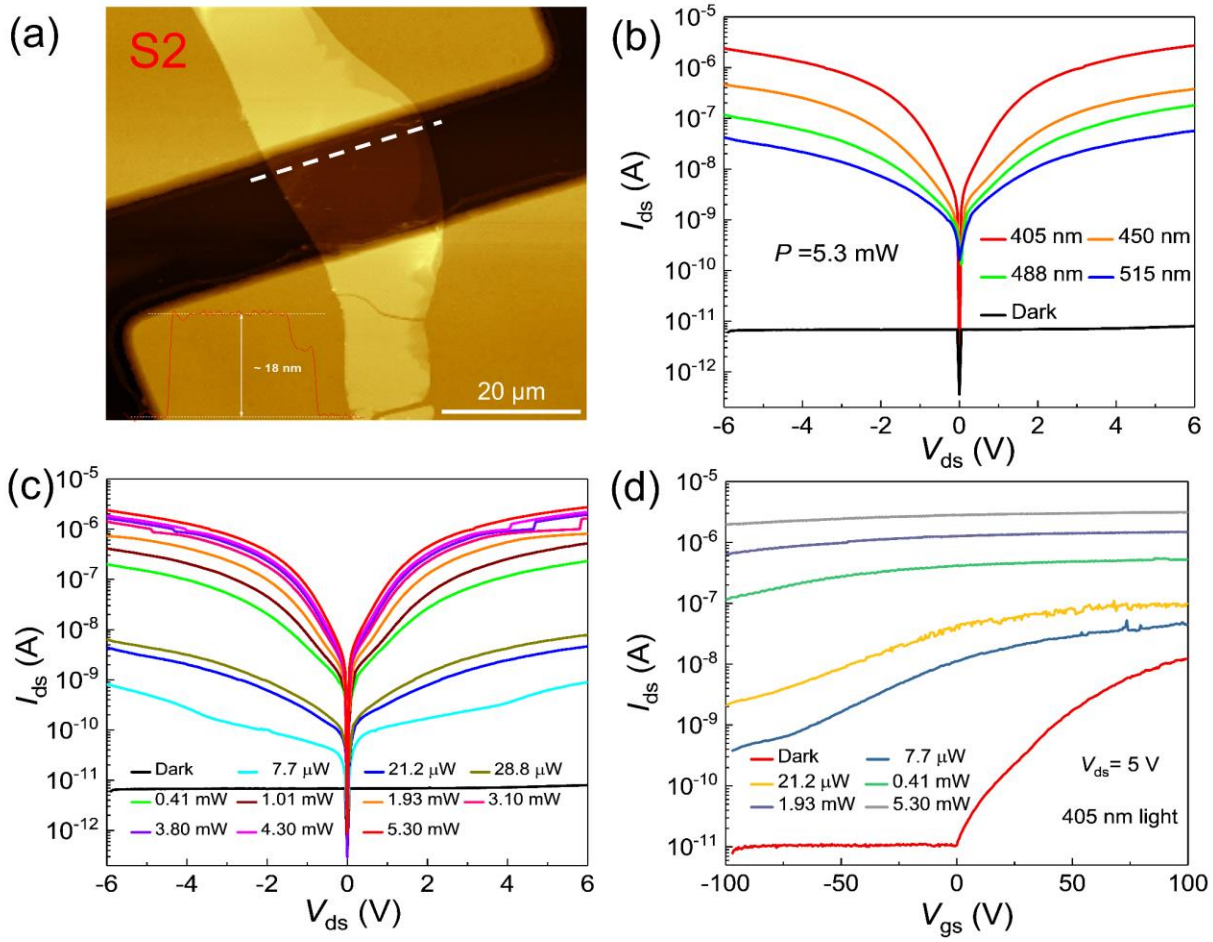

Figure S9. (a) AFM image of device S2. The thickness of R-ZIS flake is about 18 nm. The scale bar is 20 μm. (b) Semi-logarithmic I_{ds}–V_{ds} curves taken in the dark and under illumination of different wavelengths. The laser power is tuned to 5.3 mW. (c) I_{ds}–V_{ds} curves taken in the dark and under a 405 nm laser tuned to different powers. (d) Transfer curves at V_{ds} = 5 V under the 405 nm laser.

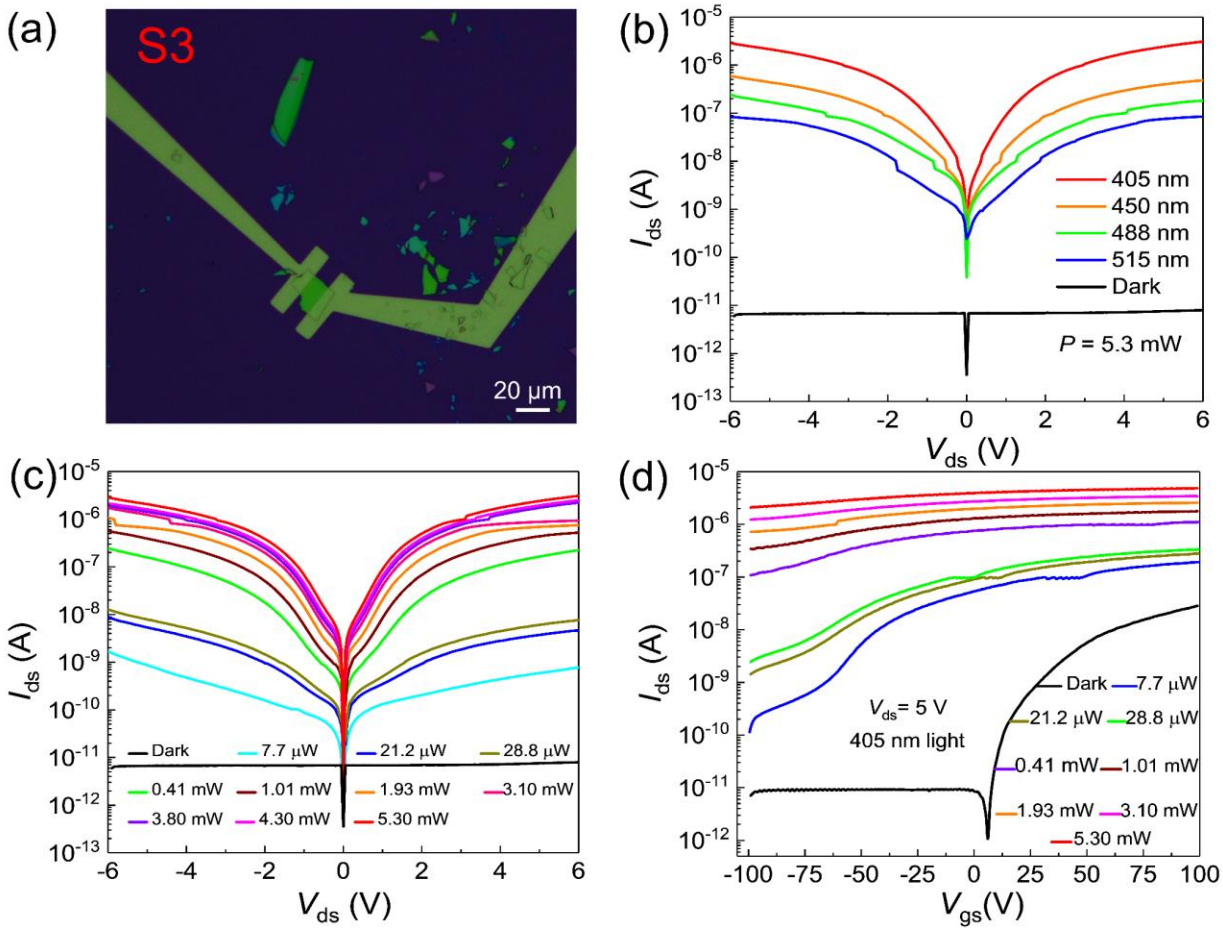

Figure S10. (a) Optical image of device S3. The scale bar is 20 μm. (b) Semi-logarithmic I_{ds}–V_{ds} curves taken in the dark and under illumination of different wavelengths. The laser power is tuned to 5.3 mW. (c) I_{ds}–V_{ds} curves taken in the dark and under a 405 nm laser tuned to different powers. (d) Transfer curves at V_{ds} = 5 V under the 405 nm laser.

1.10. Diagram of optoelectronic measurement setup

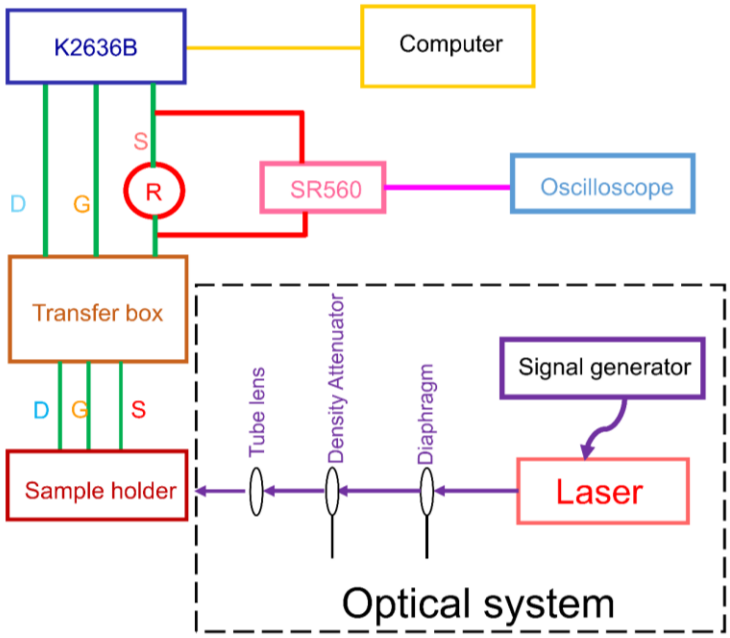

Figure S11. Diagram of optoelectronic measurement setup. The incident laser is produced by a fiber-coupled laser and the frequency of the laser can be changed by an external arbitrary signal generator (Tektronix AFG31021). The power of illumination laser is determined by a power and energy meter (Laser Power Meter LP10, Sanwa), and electrodes of the device are connected to a semiconductor device analyzer (Keithley 2636B) equipped with a homemade transfer box. The current signal is converted to a voltage signal using a resistance box, and then the voltage signal is passed to the preamp (Stanford Research System, SR560). Finally, the output voltage (from SR560) is displayed on an oscilloscope (Tektronix MDO3014).

1.11. Comparison of photoresponse characteristics of R-ZIS with some reported photodetectors based on 2D materials

Table S1. Comparison of photoresponse characteristics of ZIS with some reported photodetectors based on 2D materials.

Material	Laser (nm)	V_{bias} (V)	V_g (V)	I_{dark} (nA)	R (A W^{-1})	D^* (Jones)	τ_{rise} (ms)	τ_{decay} (ms)
InSe[1]	450	10	70	2000	157	$<10^{12}$	50	4×10^{3}
$ReSe_2$[2]	633	0.5	0	2.5	95	-	68	34
SnS_2[3]	350	1	20	525	400	-	20	16
GaSe[4]	380	4	0	0.5	2.6	1.0×10^{12}	2.37×10^{4}	6.3×10^{3}
Si_2Te_3[5]	450	1	40	0.08	27	2.8×10^{12}	210	478
$NiPS_3$[6]	245	10	0	$<10^{-5}$	0.13	1.2×10^{12}	3.2	17.2
$MnPS_3$[7]	365	8	70	1.4×10^{-3}	288	6.48×10^{11}	340	600
Ta_2NiSe_5[8]	808	0.1	0	4500	17.21	-	3000	3300
$Ga_2In_4S_9$[9]	360	5	0	0.5	112	2.25×10^{11}	40	50
R-$ZnIn_2S_4$ (This work)	405	5	0	7×10^{-3}	230	1.8×10^{14}	0.22	0.158
R-$ZnIn_2S_4$ (This work)	405	5	70	66	1.0×10^{4}	3.7×10^{13}	0.75	0.536

1.12. Correlation coefficients between the theoretical results and the outputs combining R-ZIS photodetector *I–V* characteristics

Table S2. Correlation coefficients between the theoretical results and the outputs combining ZIS photodetector *I–V* characteristics.

Map number	Kernel 1	Kernel 2	Kernel 3
II	0.8192	0.9175	0.8773
III	0.9449	0.9655	0.9564
IV	0.9598	0.9769	0.9648
V	0.9677	0.9813	0.9767

2. Reliability of using TEM to identify atoms in thin flakes

Aberration-corrected scanning transmission electron microscopy (STEM) is an effective tool for characterizing thin-flake samples at the atomic scale. In previous researches, few-layer or monolayer 2D materials were indeed unstable or even damaged under high-energy electron beams with acceleration voltages over 120 kV [PRL, 109, 035503 (2012), Ultramicroscopy 146, 33 (2014)]. However, by lowering the acceleration voltage, typically below 100 kV, the damage caused by the electron beam to the materials can be reduced, allowing the identification of atoms and defects in thin materials. This has been achieved in many few-layer and monolayer 2D materials, such as MoS_2 [Adv. Mater. 26, 2857 (2014), Adv. Mater. 26, 2648 (2014)], WSe_2 [Chem. Mater. 33, 1307 (2021), Adv. Mater. 2022, 2106551, Nat. Phys. 17, 92 (2021)], $MoTe_2$ [ACS Nano 11, 11005 (2017)], InSe [ACS Nano 13, 5112 (2019)], GaSe [ACS Nano 9, 8078 (2015)] and ReS_2 [ACS Nano 9, 11249 (2015)]. These results demonstrate the reliability of this identification.

In addition, for the monolayer and few-layer hexagonal phase $ZnIn_2S_4$, an isomer of rhombohedral $ZnIn_2S_4$ in the present work, the identification of atoms and Zn vacancies by STEM has been successfully performed [JACS 139, 7586 (2017), ACS Nano 15, 15238 (2021),

ChemSusChem 14, 852 (2021)]. Based on these experiences, we chose a relatively low acceleration voltage of 80 kV in the STEM experiment, which reduced the damage to the sample and gave satisfactory results. Therefore, the STEM characterization and analysis presented in Figure 2 are reliable.

3. Noise current and dark current

According to previous studies [Science 325,5948 (2009)], the total noise of photodetectors operating in DC and low frequency modes consists of two main components, thermal noise and shot noise. The shot noise originates from dark current. Their contributions can be estimated by calculations using the following parameters, I_{dark} = 7 pA, V_{ds} =5 V and T = 300 K.

The thermal noise is calculated as

$$i_{thermal}=\sqrt{\frac{4k_BT}{R}}=\sqrt{\frac{4\times1.38\times10^{-23}\times300}{7.14\times10^{11}}}\ \mathrm{A\ Hz^{-1/2}}=1.52\times10^{-16}\ \mathrm{A\ Hz^{-1/2}},$$

where k_B is the Boltzmann constant and R is the channel resistance of the device.

The shot noise is calculated as

$$i_{shot}=\sqrt{2eI_{dark}}=\sqrt{2\times1.6\times10^{-19}\times7\times10^{-12}}\ \mathrm{A\ Hz^{-1/2}}=1.5\times10^{-15}\ \mathrm{A\ Hz^{-1/2}},$$

where e is the elementary charge.

Thus, the total noise current is

$$i_{total}=\sqrt{i_{thermal}^2+i_{shot}^2}=\sqrt{(1.52\times10^{-16})^2+(1.5\times10^{-15})^2}\ \mathrm{A\ Hz^{-1/2}}=1.507\times10^{-15}\ \mathrm{A\ Hz^{-1/2}}\approx i_{shot}.$$

From the calculations, it is found that the shot noise is one order of magnitude larger than the thermal noise. The shot noise is the major contribution to the total noise. Therefore, it is reasonable and safe to use I_{dark} instead of the total noise current to calculate D^*.

1. Tamalampudi, S. R.; Lu, Y. Y.; Kumar, U. R.; Sankar, R.; Liao, C. D.; Moorthy, B. K.; Cheng, C. H.; Chou, F. C.; Chen, Y. T. High Performance and Bendable Few-Layered InSe Photodetectors with Broad Spectral Response *Nano Lett.* **2014,** *14*, 2800-2806.

2. Yang, S.; Tongay, S.; Li, Y.; Yue, Q.; Xia, J. B.; Li, S. S.; Li, J.; Wei, S. H. Layer-Dependent Electrical and Optoelectronic Responses of ReSe2 Nanosheet Transistors *Nanoscale* **2014,** *6*, 7226-7231.

3. Xia, J.; Zhu, D.; Wang, L.; Huang, B.; Huang, X.; Meng, X.-M. Large-Scale Growth of Two-

Dimensional SnS2 Crystals Driven by Screw Dislocations and Application to Photodetectors *Adv. Funct. Mater.* **2015,** *25*, 4255-4261.
4. Sorifi, S.; Moun, M.; Kaushik, S.; Singh, R. High-Temperature Performance of a GaSe Nanosheet-Based Broadband Photodetector *ACS Appl. Electron. Mater.* **2020,** *2*, 670-676.
5. Chen, J.; Tan, C.; Li, G.; Chen, L.; Zhang, H.; Yin, S.; Li, M.; Li, L.; Li, G. 2D Silicon-Based Semiconductor Si2Te3 toward Broadband Photodetection *Small* **2021,** *17*, 2006496.
6. Chu, J.; Wang, F.; Yin, L.; Lei, L.; Yan, C.; Wang, F.; Wen, Y.; Wang, Z.; Jiang, C.; Feng, L.; Xiong, J.; Li, Y.; He, J. High-Performance Ultraviolet Photodetector Based on a Few-Layered 2D NiPS3 Nanosheet *Adv. Funct. Mater.* **2017,** *27*, 1701342.
7. Kumar, R.; Jenjeti, R. N.; Austeria, M. P.; Sampath, S. Bulk and Few-Layer MnPS3: a New Candidate for Field Effect Transistors and UV Photodetectors *J. Mater. Chem. C* **2019,** *7*, 324-329.
8. Li, L.; Wang, W.; Gan, L.; Zhou, N.; Zhu, X.; Zhang, Q.; Li, H.; Tian, M.; Zhai, T. Ternary Ta2NiSe5 Flakes for a High-Performance Infrared Photodetector *Adv. Funct. Mater.* **2016,** *26*, 8281-8289.
9. Wang, F.; Gao, T.; Zhang, Q.; Hu, Z. Y.; Jin, B.; Li, L.; Zhou, X.; Li, H.; Van Tendeloo, G.; Zhai, T. Liquid-Alloy-Assisted Growth of 2D Ternary Ga2In4S9 toward High-Performance UV Photodetection *Adv. Mater.* **2019,** *31*, 1806306.